



Nanocrystallization enabled tensile ductility of Co-based amorphous microwires

Huan Wang,^{a,b} Dawei Xing,^a Huaxin Peng,^{b,c} Faxiang Qin,^b Fuyang Cao,^a Guoqiang Wang^a and Jianfei Sun^{a,*}

^aSchool of Materials Science and Engineering, Harbin Institute of Technology, Harbin 150001, People's Republic of China

^bAdvanced Composite Center for Innovation and Science (ACCIS), Department of Aerospace Engineering, University of Bristol, University Walk, Bristol BS8 1TR, UK

^cBristol Centre for NanoScience and Quantum Information (NSQI), University of Bristol, University Walk, Bristol BS8 1TR, UK

Received 1 February 2012; revised 9 February 2012; accepted 10 February 2012

Melt-extracted amorphous $\text{Co}_{68.15}\text{Fe}_{4.35}\text{Si}_{12.25}\text{B}_{15.25}$ microwires were drawn at ambient temperature into different diameters and the dependence of tensile properties and microstructural evolution on the degree of deformation was investigated. The cold-drawn wire with 51% area cross-section reduction exhibits a tensile ductility of 1.64%, with a tensile strength exceeding 4000 MPa. Deformation-induced Co-rich nanocrystals were observed in the cold-drawn wires and proved to be capable of arresting the quick extension of shear bands and leading to the enhanced global plasticity of the microwires.

© 2012 Published by Elsevier Ltd. on behalf of Acta Materialia Inc.

Keywords: Amorphous wire; Melt extraction; Cold drawing; Tensile ductility; Microstructure evolution

Due to their unique mechanical and physical properties afforded by the disordered atomic arrangement, amorphous alloys have attracted great attention from both the scientific and industrial communities [1,2]. However, the industrial applications of such alloys have been hindered by their limited plastic deformability, especially their near zero tensile plasticity at room temperature resulting from the formation of highly localized shear bands [3,4]. In another perspective, when the sample size is reduced to the micro- or nanoscale, there have been considerable improvements in their mechanical properties [5–8]. It has been reported that shear bands could even be completely suppressed when the sample size was at submicron scale, leading to a homogeneous deformation at room temperature.

Recently, a variety of pre-treatments, such as shot peening, channel die compression, cold rolling and drawing, have been shown to effectively improve the plastic deformability of amorphous alloys [9–12]. The effect of cold drawing on the mechanical properties of Pd-based and Fe-based amorphous wires produced by the in-rotating-water spinning method was investigated by Takayama [13] and Hagiwara et al. [14]. It was

shown that the drawn wire exhibited a fracture stress that is 5–8% larger than that of undrawn wire with a plastic strain of 0.7%. The authors attributed this phenomenon to the prevention of further deformation through the interaction between numerous shear bands in pre-deformed areas. Wu et al. [12] reported an improvement in the tensile fracture strength of cold-drawn Co-based in-rotating-water spinning wire by removing surface flaws and generating compressive residual stress, which also led to an improvement of its fracture reliability.

It is clear that, for metallic microwires, the early research tended to focus on the generation of multiple shear bands and the removal of surface flaws to prevent the sudden crack initiation and propagation, while neglecting the microstructure evolution during the pre-treatment and deformation process. The relationship between the tensile properties and the microstructural changes during deformation, and the mechanism for the formation of these deformation-induced heterogeneous microstructures as well as their role in the plastic deformation of these micro-sized samples, are not well understood. In the present work, CoFeSiB amorphous microwires fabricated by a modified melt extraction method were cold-drawn into various diameters. The effect of cold drawing on the mechanical property and microstructural evolution as well as the mechanism of

* Corresponding author. Tel.: +86 451 8641 8317; fax: +86 451 8641 3904.; e-mail: jfsun_hit@263.net

nanocrystallite formation during drawing were investigated systematically.

Quaternary master alloy ingot with nominal composition of $\text{Co}_{68.15}\text{Fe}_{4.35}\text{Si}_{12.25}\text{B}_{15.25}$ was prepared by arc-melting pure Co (99.99%), Fe (99.9%), Si (99.99%) and B (99.7%) in an argon atmosphere. The alloy ingot was completely remelted and sucked into a copper mould with a diameter of 8 mm. A continuous near-circular CoFeSiB wire with a diameter of about 60 μm was fabricated by a modified melt extraction method [15]. The diameter of the extracted wire was reduced step by step through a number of drawing processes using diamond dies without any intermittent annealing. Details of how to cold draw metallic wires have been described elsewhere [12,14]. The cross-section area reduction ratio, R was controlled within 4% at each step. The microwire diameter was reduced from around 60 μm down to 30 μm . Tensile samples were prepared conforming to the ASTM standard D3379-75 with a gauge length of 10 mm. Uniaxial microtension experiments and cyclic loading tests were conducted using a dynamic mechanical analyzer (DMA Q800) with a loading rate of 0.5 N min^{-1} , and at least eight samples were tested for each type of wires. The fracture morphology was examined using scanning electron microscopy (SEM). Transmission electron microscopy (TEM) specimens were prepared by ion milling operated at an ion beam energy level of 4.5 keV and the microstructure change before and after cold drawing were examined using a Tecnai G² F30 high-resolution transmission electron microscope at 300 kV. The thermal properties associated with glass transition and crystallization were evaluated by differential scanning calorimetry (DSC; Perkin-Elmer) under a flowing argon atmosphere at a heating rate of 20 K min^{-1} .

$\text{Co}_{68.15}\text{Fe}_{4.35}\text{Si}_{12.25}\text{B}_{15.25}$ metallic wires were easily drawn to 75% reduction in area without breakage. Figure 1(a) shows the stress–strain curves during microtension tests for wires with $R = 0\%$, 51% and 75%, with an offset of 1% strain. It can be seen that the as-cast wire shows near-zero tensile plasticity with a fracture strength of about 3433 MPa. This is consistent with early experimental observations for Co-based glass-covered amorphous wires [16]. The stress–strain curves for cold-drawn wires show typical plastic deformation and especially, the 51% cold drawn wire exhibits a rather high fracture strength exceeding 4000 MPa. The early departure from elastic linearity ascribed to apparent yield stress or flow stress (the arrows indicated in Fig. 1(a)) was observed. With increasing R value, the plastic elongation as well as fracture strength first increased, then decreased. The maximum tensile plastic strain obtained with 51% cold-drawn microwire was 1.63%, considerably higher than those reported values in the open literature. A typical fracture surface image of the 51% drawn-wire is shown in Figure 1(b). It is important to note that no shear band step was observed on the surface in the fracture region during the tensile test, indicating that shear bands induced by tensile loading are somewhat limited and consequently do not contribute much to the overall tensile plasticity. The inset in Figure 1(b) shows a high magnification image of the vein pattern of the 51% drawn wire with a smooth tearing morphology and a viscous-like deformation, clearly indicating the activation of flow processes.

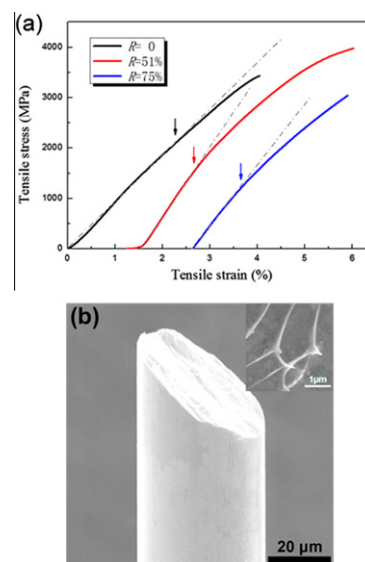


Figure 1. (a) Typical stress–strain curves of the as-cast and cold-drawn Co-based microwires. (b) Fracture morphology of 51% cold-drawn microwire exhibiting 1.63% tensile plasticity and (inset) a high-magnification view of its vein pattern.

The microstructure identified by the high-resolution transmission electron microscopy (HRTEM) is shown in Figure 2 for the three different samples: as-cast, 51% cold-drawn and 75% cold-drawn wire. No contrast or obvious lattice fringe can be detected in Figure 2(a), demonstrating the full amorphous nature of the as-cast wire. Figure 2(b) shows the HRTEM image of the 51% drawn sample. Isolated nanocrystallites with an average size of 4 nm were distributed homogeneously in the amorphous matrix. Such a microstructure was also reported recently by Branagan et al. [17,18] in glass-covered Fe-based amorphous matrix composite wire through spinodal decomposition, yielding tensile ductility up to 8% with strengths up to 4.8 GPa. For the $R = 75\%$ sample, the size of these nanocrystals become larger, with diameter of more than 10 nm, and connected with each other. The inverse fast Fourier transform (IFFT) patterns of

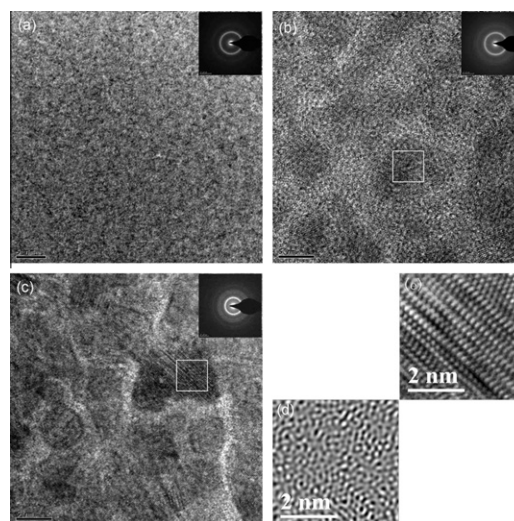


Figure 2. HRTEM images of the (a) as-cast, (b) 51% cold-drawn and (c) 75% cold-drawn wires. IFFT patterns of nanocrystals, marked by rectangles in (b) and (c), are shown in (d) and (e), respectively.

the 51% and 75% cold-drawn nanocrystals, marked by rectangles in Figure 2(b) and (c), are shown in Figure 2(d) and (e), respectively. It is shown that the degree of localized ordering is low for the 51% drawn wire, with small crystallized regions embedded in the residual amorphous matrix, while a crystallized structure was observed in Figure 2(e) for the 75% drawn sample. The coexistence of dislocation and distortion of lattice in the larger deformed materials will degrade its mechanical performance. The crystal structure of these nanoscale precipitations cannot be identified due to their small size, while a Co-rich phase with an average composition of $\text{Co}_{90.69}\text{Fe}_{5.44}\text{Si}_{3.87}$ (B element is not included here) can be identified from the energy-dispersive spectrum analysis relative to the normal composition.

In order to further study the structural change during drawing, a DSC test was performed, as shown in Figure 3. The as-cast wire exhibits an endothermic event, characterized by a glass transition temperature $T_g = 730$ K, followed by a crystallization event at $T_x = 818$ K. With the area reduction increasing further, all samples exhibit similar DSC traces and the first crystallization peak temperature remains constant, not shifting with the temperature. However, the glass transition temperature T_g becomes blurred and the heat release calculated from the DSC scan decreases with increasing area reduction. These observations indicate that the amount of amorphous phase decreases with the drawing process and nanocrystallization occurred during cold drawing, which is consistent with the HRTEM observation presented in Figure 2.

The high tensile strength and distinct tensile plasticity observed in the cold-drawn microwires with $R = 51\%$ prompted us to probe its nonlinear tensile deformation in more detail. As shown in Figure 4, multiple loading–unloading cycles were conducted. One can see that, below the flow stress, the unloaded curve can return to the starting point, while, with the applied stress exceeding the flow stress, the strain cannot return to zero, and shows typical nonlinear deformation behavior. Of particular importance is that the tensile strain shows nonlinear hysteretic behavior at the same time, as indicated by the arrow in Figure 4. That is, when the reload stress reaches the last unloading point, the corresponding strain is larger than the previous unloading curve, and the interval of strain increases monotonically with increasing cycle count. It can also be seen that the elastic modulus increases monotonically with increasing

number of reload cycles. This is likely due to the increasing volume fraction of nanocrystallites within the sample. The volume fraction and the elastic modulus of nanocrystals can be estimated by a uniform stress model, i.e. the lower bound of the rule of mixture [19]:

$$1/E_c = f_n/E_n + (1 - f_n)/E_a \quad (1)$$

where E_c , E_n and E_a are the Young's modulus of composite, nanocrystal and amorphous phase, respectively. f_n is the volume fraction of nanocrystal. E_c was measured to be 148.5 GPa according to the traditional DMA test, and E_a was identified as 131 GPa for the CoFeSiB amorphous wire [16]. The volume fraction f_n was measured to be about 0.20 by HRTEM in Figure 2(b), and thus E_n was calculated approximately as 318.9 GPa. The Young's moduli tested during the cyclic tensile experiment are 157.68 ± 0.334 , 162.49 ± 0.955 , 175.7 ± 1.89 and 180.2 ± 3.27 GPa, respectively. The nanocrystallization fraction of each loading can be calculated approximately as $28.7 \pm 0.3\%$, $32.9 \pm 0.8\%$, $43.2 \pm 1.4\%$ and $48.5 \pm 2.2\%$ following Eq. (1). The nanocrystallization generated during the tensile test is also likely to be related to its large ductility and strain hardening, analogous to the cold drawing process.

We now discuss the formation mechanism during mechanical deformation. Since amorphous alloys are fabricated by rapid solidification technology, the chemistry and stress distribution are not perfectly uniform in the as-cast condition. These inhomogeneities act as nucleation sites of nanocrystallites to promote the transformation under external stress. The relationship between the change in the energy barrier for nucleation (ΔG^*) required to form a critical sized nucleus and the hydrostatic pressure (P) can be expressed as follows [20]:

$$\left(\frac{\partial(\Delta G_m^*)}{\partial P}\right)_T = -\frac{64\pi\gamma^3}{3} \frac{\Delta V}{(\Delta G_m + E + P\Delta V)} \quad (2)$$

where ΔG_m is the molar free energy change, i.e. the driving force, for an amorphous-to-crystalline phase transformation, E is the elastic energy induced by a volume change during the phase transformation, γ is the interfacial free energy between the crystalline and the amorphous phases, and ΔV is the volume change associated with the formation of a crystalline nucleus. The values for ΔG_m and ΔV are both negative and the elastic strain energy (E) is rather low and can be ignored. Therefore, the value of $(\partial(\Delta G_m^*)/\partial P)_T$ is also negative, indicating that the energy barrier for nanocrystallites nucleation

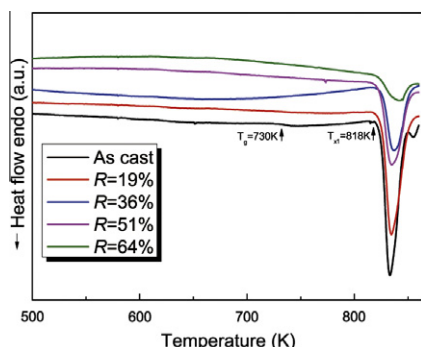


Figure 3. Differential scanning calorimetry (DSC) curves for different wires.

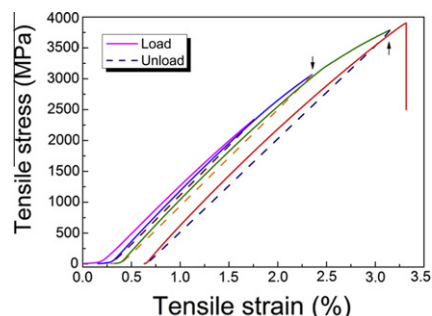


Figure 4. Typical stress–strain curve with four loading–unloading cycles of the 51% cold-drawn wire.

decreases with increasing hydrostatic pressure. When the amorphous wires were drawn within the diamond die, compressive stresses were generated along the radius direction, resulting in an amorphous-to-nanocrystalline phase transformation.

Recently, the mechanism of shear-band-formation-induced nanocrystallization has been investigated by in situ transmission electron microscopy [21,22]. The results show that the most important influencing factor for these nanocrystallization behaviors is not the maximum temperature induced by deformation, but the time that the heated volume stays at an elevated temperature, even though the time at elevated temperature is less than 1 μ s. Compared with other bulk metallic glass compositions, rapidly solidified CoFeSiB alloy has poor glass-forming ability and often contains chemistry and stress heterogeneity, acting as nucleation sites of nanocrystals during the subsequent drawing process. Previous studies have suggested that the activation energy for nucleation is greater than the activation energy for crystal growth in amorphous alloys [21–23]. In our test, for large deformation ($R = 75\%$), once small-sized nanocrystals are introduced (after 51% cold drawing), the time at which the material is elevated above T_x may be adequate for crystal growth but is insufficient for new nanocrystal nucleation, so the formation of larger crystals is therefore easier to facilitate for the 75% cold-drawn samples.

Another factor that can accelerate this phase transformation is the tensile stress during the DMA test, as shown in Figure 4. A change in the elastic modulus during cyclic loading is indirect evidence of a microstructure change in the tensile process. Compared with other Zr-based [24], Pd-based [13], Ni-based [25] and Co-based amorphous microwires [8,12], the 51% cold-drawn microwire in the present study exhibits the largest fracture energy absorption, characterized by the area under the curve. This increases the energy state of the amorphous matrix, which in turn leads to an increase in the driving force (ΔG_m) for the amorphous-to-crystalline phase transformation.

It is important for the amorphous alloys with high mechanical performances that the free propagation of active shear bands are constrained or the energy that accelerates its expansion is dissipated. As pointed out by Hofmann et al. [26], the large tensile plasticity of bulk amorphous alloy composite is based on two principles: (i) introducing soft elastic/plastic inhomogeneities into an amorphous matrix to initiate local shear banding around the inhomogeneities; and (ii) matching microstructural length scales to the characteristic length scale for plastic shielding of an opening crack tip to limit shear band extension, suppress shear band opening and avoid crack development. In the present study, mechanically induced nanocrystallites with a diameter of less than 5 nm precipitated in melt-extracted Co-based microwires after 51% cold drawing. The inhomogeneous structure with isolated nanocrystallites in the amorphous matrix can stabilize the sample against the catastrophic failure and arrest the rapid extension of the shear band, resulting in enhanced global plasticity.

In summary, the effect of cold drawing on the mechanical properties and microstructural evolution of wires was investigated systematically. Tensile plasticity and tensile strength increased after cold drawing and

reached a peak at 51% cross-section area reduction. The 51% cold-drawn wire exhibits a tensile strength exceeding 4000 MPa and a tensile strain of 1.634% at room temperature. Nanosized crystallites induced by cold drawing and the tensile process can dissipate the elastic strain energy, stabilize the shear bands and arrest its rapid propagation, leading to enhanced global plasticity. The cold-drawn wires are promising as a new engineering material with ultrahigh strength and good plasticity for microwire-reinforced resin matrix composites and microelectromechanical systems application.

The authors are grateful for the financial support from the Doctoral Visiting Scholar Program of Harbin Institute of Technology. They also acknowledge useful discussions with Junwei Qiao from Taiyuan University of Technology, DongDong Qu, Yongjiang Huang and Lunyong Zhang from the Harbin Institute of Technology.

- [1] W. Wang, *Adv. Mater.* 21 (2009) 4524.
- [2] A.L. Greer, *Science* 267 (1995) 1947.
- [3] N. Nishiyama, K. Amiya, A. Inoue, *Mater. Trans.* 45 (2004) 1245.
- [4] C.A. Schuh, T.C. Hufnagel, U. Ramamurty, *Acta Mater.* 55 (2007) 4067.
- [5] Q. Zheng, S. Cheng, J. Strader, E. Ma, J. Xu, *Scripta Mater.* 56 (2007) 161.
- [6] H. Guo, P. Yan, Y. Wang, J. Tan, Z. Zhang, M. Sui, E. Ma, *Nat. Mater.* 6 (2007) 735.
- [7] Q. Deng, Y. Cheng, Y. Yue, L. Zhang, Z. Zhang, X. Han, E. Ma, *Acta Mater.* 59 (2011) 6511.
- [8] Y. Wu, H.X. Li, G.L. Chen, X.D. Hui, B.Y. Wang, Z.P. Lu, *Scripta Mater.* 61 (2009) 564.
- [9] A. Concustell, F. Mear, S. Surinach, M. Baro, A. Greer, *Phil. Mag. Lett.* 89 (2009) 831.
- [10] Y. Zhang, W. Wang, A. Greer, *Nat. Mater.* 5 (2006) 857.
- [11] M. Lee, K. Lee, J. Das, J. Thomas, U. Khn, J. Eckert, *Scripta Mater.* 62 (2010) 678.
- [12] Y. Wu, H.H. Wu, X.D. Hui, G.L. Chen, Z.P. Lu, *Acta Mater.* 58 (2010) 2564.
- [13] S. Takayama, *Mater. Sci. Eng.* 38 (1979) 41.
- [14] M. Hagiwara, A. Inoue, T. Masumoto, *Metall. Mater. Trans. A* 13 (1982) 373.
- [15] H. Wang, D. Xing, X. Wang, J. Sun, *Metall. Mater. Trans. A* 42A (2010) 1103.
- [16] H. Chiriac, T.A. Ovari, *Prog. Mater. Sci.* 40 (1996) 333.
- [17] D. Branagan, J. Zhou, B. Meacham, A. Sergueeva, *Adv. Mater. Processes* 168 (2010) 25.
- [18] A. Sergueeva, J. Walleiser, J. Zhou, B. Meacham, D. Branagan, *Mater. Sci. Eng., A* 534 (2012) 603.
- [19] K.S. Ahmed, S. Vijayarangan, A.C.B. Naidu, *Mater. Des.* 28 (2007) 2287.
- [20] S.-W. Lee, M.-Y. Huh, E. Fleury, J.-C. Lee, *Acta Mater.* 54 (2006) 349.
- [21] D. Matthews, V. Ocelik, P. Bronsveld, J.T.M. De Hosson, *Acta Mater.* 56 (2008) 1762.
- [22] J.R. Greer, J.T.M. De Hosson, *Prog. Mater. Sci.* 56 (2011) 654.
- [23] K. Lu, J. Wang, *Mater. Sci. Eng., A* 133 (1991) 500.
- [24] J. Yi, X. Xia, D. Zhao, M. Pan, H. Bai, W. Wang, *Adv. Eng. Mater.* 12 (2010) 1117.
- [25] A. Inoue, Y. Masumoto, N. Yano, A. Kawashima, K. Hashimoto, T. Masumoto, *J. Mater. Sci.* 20 (1985) 97.
- [26] D.C. Hofmann, J.-Y. Suh, A. Wiest, G. Duan, M.-L. Lind, M.D. Demetriou, W.L. Johnson, *Nature* 451 (2008) 1085.